Michelini *et al. Int J Concr Struct Mater* (2020) 14:31
https://doi.org/10.1186/s40069-020-00407-y

International Journal of Concrete Structures and Materials

RESEARCH Open Access

Experimental and Numerical Assessment of Flexural and Shear Behavior of Precast Prestressed Deep Hollow-Core Slabs

E. Michelini*, P. Bernardi, R. Cerioni and B. Belletti

Abstract

The paper presents the results of flexural and shear tests up to failure on full-scale hollow-core slabs (HCS) having a depth of 500 mm. A detailed non-linear 2D finite element model is also developed to predict the stress distribution and crack pattern within the slabs, providing a well match with experimental results. Experimental and numerical results are compared with analytical calculations provided by Product Standard EN 1168, highlighting the inaccuracy of technical regulations in predicting shear behavior. The proposed numerical procedure is instead viable and sound for the design and the strength assessment of HCS, and can be extended easily to the analysis of whole floor systems.

Keywords: hollow-core slabs, prestressed concrete, precast concrete, full-scale tests, non-linear finite element analysis, cracking, shear strength, flexural strength, fracture mechanics

1 Introduction

Precast prestressed Hollow-Core Slabs (HCS) are widely used for floors and roofs in commercial and industrial buildings, since they represent an economic and flexible solution. As floor units, HCS structures perform very well despite their limited weight, allowing to cover long spans and offering several advantages in comparison with conventional concrete members, like high quality control, low onsite labor costs and short construction times (CEB-FIP 2000; Derkowski and Surma 2015b; Elliot, 2002; Nguyen et al. 2019; Park et al. 2019; Rahman et al. 2012). As roof units, HCS are typically used in conventional prefabricated constructions (Belleri et al. 2015; Savoia et al. 2017), sometimes in combination with composite steel beams (Hegger et al. 2009; Lam et al. 2000), and represent a good alternative to other special covering solutions, like thin-webbed precast elements (Belletti et al. 2015; Bernardi et al. 2020; Dal Lago 2017).

The diaphragm action is obtained by connecting HCS to each other and to the framing beams through cast-in place Reinforced Concrete (RC) joints, which allow for transverse load redistribution within the floor (Bernardi et al. 2016a; Lundgren et al. 2004; Song et al. 2009). In seismic areas, the upper surface of precast slabs can be leveled with a cast in situ concrete topping, so to enhance the structural performance of the floor under lateral loads. Anyway, an effective composite action can be achieved only when the topping has an adequate thickness, and when a proper shear strength is provided at the interface between the topping itself and the slabs (Baran 2015; Derkowski and Surma 2015a; Girhammar and Pajari 2008; Ibrahim et al. 2016; Ueda and Stitmannaithum 1991).

The robustness of prefabricated structures against progressive collapse caused by unforeseen events (like column removal induced by explosions, impacts, etc.) is still under investigation and require experimental and numerical researches when HCS are used to realize the diaphragm system (Belletti et al. 2019).

HCS are usually designed as simply supported elements subjected to bending, but their specific features make them more sensitive than other structures to

*Correspondence: elena.michelini@unipr.it
Department of Engineering and Architecture, University of Parma, Parco Area delle Scienze 181/A, 43124 Parma, Italy
Journal information: ISSN 1976-0485 / eISSN 2234-1315

shear and torsion (Broo et al. 2007; Brunesi et al. 2015; Brunesi and Nascimbene 2015; El-Sayed et al. 2019; Pajari 2005; Palmer and Schultz 2011; Tawadrous and Morcous 2018; Walraven and Mercx 1983; Yang 1994). Their specific characteristics lie above all in the geometry of their cross-section and in the reinforcement arrangement. In order to reduce the slab weight, continuous voids, separated from each other by thin concrete webs, are realized within the cross-section, by means of extrusion or slip-forming methods. Since the production process precludes the use of typical shear reinforcement (i.e. stirrups), each slab is reinforced only by straight prestressing strands, which are usually placed at the bottom of HCS between the voids, and sometimes also at the top of the slab. Therefore, HCS show the same efficiency of other prestressed members in terms of deflection control, span range and load capacity when considering bending behavior, while the lack of transverse reinforcement makes their structural response more complex in presence of shear stresses. The shear resistance of HCS relies indeed entirely on the tensile strength of the medium–high strength concrete used for casting. Previous studies have highlighted that this type of material behaves differently with respect to normal strength concrete, due to the formation of smoother cracks, and to the consequent reduction of aggregate interlock contribution (Brunesi and Nascimbene 2015; Duthinh 1999; Pisanty and Regan 1991).

Shear strength assessment of HCS is not so straightforward also because current design approaches included in Standard Codes are based on experimental researches performed mainly on structural elements different from HCS (i.e. beams), and usually cast with normal strength concrete (Brunesi and Nascimbene 2015; Palmer and Schultz 2011). The extension of these approaches to HCS is based on elastic theories (UNI EN 1168: 2012; UNI EN 1992-1-1: 2015) and to a limited number of experimental tests specifically performed on HCS (ACI Committe 2011). Several studies (among others, e.g., Araujo et al. 2011; Belletti et al. 2003; Broo, 2008; Brunesi et al. 2015; Brunesi and Nascimbene 2015; Garutti 2013; Sgambi et al. 2014; Wang 2007) provided numerical predictions of HCS shear behavior at ultimate conditions, based on more or less sophisticated Finite Element (FE) approaches calibrated on the experimental test results available in the literature. Even if the most of the researches underlined the inadequacy of analytical formulations adopted in current design of these members for different slab types, the shear strength assessment of HCS is still an open issue and a general consensus in the academic community has not been reached yet (Araujo et al. 2011; Bertagnoli and Mancini 2009; Pajari 2009; Simasathien and Chao 2015).

This work represents a further contribution in this debate. The attention is focused on 500 mm deep HCS, which are judged to be more interesting due to their large use in the building sector and their inherently brittle behavior. Furthermore, the inaccuracy of Code provisions in predicting shear response for these elements is greater than for slim sections, characterized by circular voids. The research was structured into two phases: first the bending and shear behavior of deep HCS was experimentally assessed, by performing a total of four tests (2 in bending and 2 in shear) on full-scale specimens without concrete topping; then a numerical procedure based on fracture mechanics was developed to model their behavior up to failure. On this point it should be underlined that flexural tests, which are generally less widespread than shear ones (being bending behavior less critical, e.g., Ibrahim et al. 2008; Prakashan et al. 2017), were conceived herein with the main aim of providing a more general verification of the proposed numerical procedure, especially with regard to the simulation of concrete behavior subjected to multi-axial state of stress. The experimental response was predicted indeed through non-linear FE analyses, by simulating the mechanical behavior of RC by means of 2D-PARC constitutive model (Bernardi et al. 2016b; Cerioni et al. 2008). This model, based on a strain decomposition approach (Rots 1988), derives from PARC crack model (Belletti et al. 2001), which is based on a total strain approach. The main feature of both 2D-PARC and PARC crack models, developed on the basis of fracture mechanics concepts, is the possibility to realistically describe the progressive development of multi-axial cracking in the structural element, by taking into account several post-cracking phenomena, such as tension stiffening, dowel action, aggregate bridging and interlock. Recently, a new release of PARC crack model, named PARC_CL, has been also implemented, able to predict the non-linear behavior of RC structures subjected to cyclic loading (Belletti et al. 2017).

Numerical results were compared to experimental ones both for strength assessment and in terms of damage pattern evolution and fracture modes at failure. Numerical strength predictions were also compared with analytical formulations suggested by HC floor Product Standard (UNI EN 1168: 2012) so to provide a further insight in the discussion of their effectiveness.

2 Experimental Program

The experimental program described herein was performed within a collaboration between the University of Parma and ASSAP (Italian Prestressed Hollow Core Slabs Manufacturers Association). A total of four tests on full-scale specimens were carried out, two of them in flexure and two in shear (respectively named H50-f and H50-s

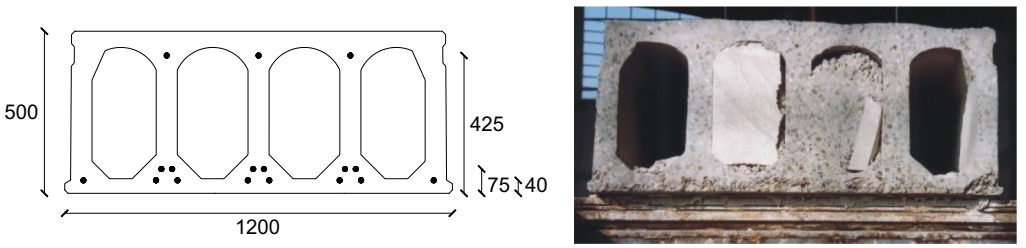

Fig. 1 **a** Sketch of the cross-section geometry and of the arrangement of prestressing reinforcement for the tested hollow core units (dimensions in mm); **b** cross-section of specimen H50-f near the supports.

Table 1 Specimens H50-f1 and H50-f2 under flexure: experimental values of concrete mechanical properties.

$f_{c,cube}$ (MPa)	$f_{c,pr}$ (MPa)[b]	$f_{c,cyl}$ (MPa)[a]	$f_{ct,sp}$ (MPa)	$f_{ct,fl}$ (MPa)[b]	$f_{ct,ax}$ (MPa)[a]
49.2	45.6	40.8	4.0	7.4	3.6

[a] Obtained from experimental values, by applying the relations suggested in Eurocode 2 (2015).

[b] Obtained by prisms extracted from the specimens.

Table 2 Specimens H50-s1 and H50-s2 under shear: experimental values of concrete mechanical properties.

$f_{c,cube}$ (MPa)	f_c (MPa)[a]	$f_{ct,sp}$ (MPa)	$f_{ct,ax}$ (MPa)[a]
54.7	45.4	4.4	4.0

[a] Obtained from experimental values, by applying the relations suggested in Eurocode 2 (2015).

in the following). A 500 mm deep HCS without concrete topping, whose cross-section is reported in Fig. 1, was tested in each case. All the specimens were manufactured by means of an extrusion machine using high-frequency vibrators and were reinforced with 17 seven wire strands, arranged in three layers (see Fig. 1a for strand location). All the strands had nominal diameter $\phi_p = 12.5$ mm (= 1/2 in.) and nominal area $A_p = 93$ mm^2, and were prestressed by applying an initial stress $\sigma_{0p} = 1350$ MPa. The mean values of experimentally measured concrete strengths are summarized in Tables 1 and 2 for the two sets of specimens, as better discussed in the following Sections. The adopted prestressing steel had a characteristic tensile strength f_{pk} of 1860 MPa and a 0.1% proof stress $f_{p0.1k}$ (as defined in Sect. 3.3 of UNI EN 1992-1-1: 2015) of 1670 MPa.

A description of the performed experimental campaign is provided in Sects. 2.1 and 2.2 for flexural and shear tests, respectively, while the obtained results are reported in Sect. 4, where they are compared with numerical outcomes.

2.1 Flexural Tests

Flexural tests were performed on two 15.30 m long simply supported specimens (denoted as H50-f1 and H50-f2), characterized by the same loading and boundary conditions. A four–point bending scheme was adopted, with two symmetric loads placed at a distance of 2.5 m from the midspan of the HC unit (Figs. 2, 3). The loads were applied by means of two hydraulic jacks, and redistributed over the slab width by means of rigid transverse steel beams (Fig. 3a). The specimen was placed over two steel supports (Fig. 3b), with a net span of 15 m. In order to prevent axial constraints, one of the steel supports was let free to slide over a Teflon layer.

According to the sketch reported in Fig. 2, three Linear Variable Displacement Transducers (LVDTs) were placed

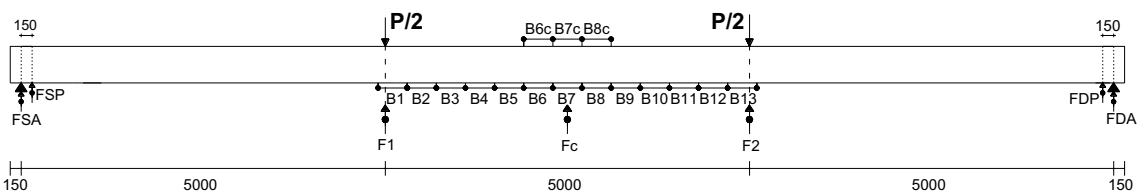

Fig. 2 Flexural tests on specimens H50-f1 and H50-f2: sketch of the loading arrangement and of the instrumentation adopted for the measuring of strains and vertical displacements (dimensions in mm).

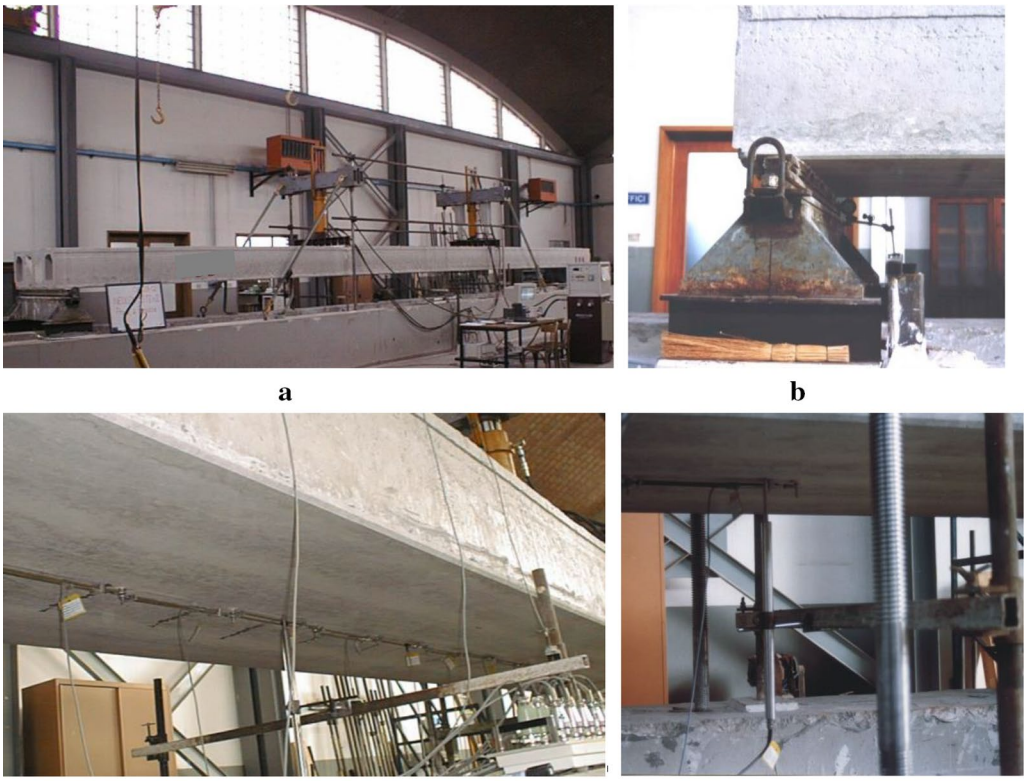

Fig. 3 Flexural tests on specimens H50-f1 and H50-f2: **a** general view of the specimen during the test; details of the adopted experimental setup: **b** steel support at specimen end; **c** LVDTs at the bottom surface of HCS; **d** LVDT for the measurement of vertical displacements.

at midspan (F_c) and in correspondence of the loaded sections (F_1 and F_2) to monitor specimen deflections (see also Fig. 3d). Dial gauges were also used to measure possible boundary movements (F_{SA}, F_{SP}, F_{DA}, F_{DP}). A total of sixteen LVDTs with a gauge length of 400 mm were adopted to evaluate concrete strains; 13 of them were placed at the bottom surface between the two loading points, in the region of maximum bending moment, while the remaining 3 were placed at the top compressed surface of the slab (Figs. 2, 3c).

The tests were carried out under loading control, by performing three loading cycles. During the 1st cycle, the load was incrementally applied until the appearance of clearly visible flexural cracks in the region of maximum moment. This load approximately corresponded to the reaching of the flexural resistant moment M_{Rd}, evaluated with material design properties. After unloading, the specimen was reloaded in a 2nd loading cycle until the appearance of new cracks. At the end of this cycle, all the instrumentation was removed for safety reasons. In the 3rd loading cycle, the load was increased until the attainment of the ultimate condition, by only monitoring midspan deflection. Figure 4 shows the load–midspan deflection curves experimentally obtained for all the performed loading cycles, for the two specimens. In the graphs, the theoretical loading levels corresponding to the reaching of cracking moment (named P_{cr}), and of the flexural resistant moments evaluated with design

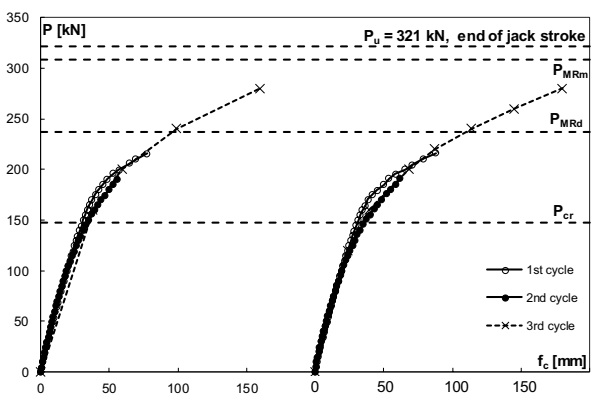

Fig. 4 Flexural tests on specimens H50-f1 and H50-f2: experimental load-midspan deflection curves for the three loading cycles.

and mean values of material properties (named P_{MRd} and P_{MRm}, respectively) are also plotted for comparison. These values are referred to the section of maximum bending moment, and are calculated by subtracting the dead load contribution, since it acted before testing. The flexural resistant moments were evaluated according to Eurocode 2 (UNI EN 1992-1-1: 2015) approach, based on sectional theory. Both the flexural tests were stopped due to the reaching of the end of jack stroke (in correspondence of a maximum load $P_{u,exp} = 321$ kN). It should be noticed that for this loading value, the slabs were characterized by very large deflections, greater than 300 mm (see Fig. 5a). Moreover, since the maximum experimental load was slightly greater than that corresponding to the flexural resistant moment evaluated with mean values of mechanical properties (P_{MRm}, see Fig. 4), this condition can be reasonably considered as the ultimate one for the panels. This seems to be also confirmed by observing the crack pattern in correspondence of maximum applied load, shown in Figs. 5b, c for both the tested specimens. As can be seen, specimen H50-f1 was characterized by the presence of a remarkable diagonal crack spreading under one of the loading points (Fig. 5b). This inclined crack appeared almost at the end of the test, after the occurring of flexural failure, and it was probably related to punching shear under the loading point, due to the large value of the applied load.

Specimen H50-f2 showed a classic flexural failure, characterized by the spreading of several vertical cracks with bifurcated branches in their upper part, which developed first between the two loading points and then in the regions between the supports and the loading points (Fig. 5c).

2.2 Shear Tests

Shear tests were performed on two identical specimens (denoted as H50-s1 and H50-s2), having a total length of 3.0 m. The specimens were simply supported over a net span of 2.8 m. Boundary conditions were the same adopted in flexural tests, and described in Sect. 2.1. The specimens were subjected to a concentrated load, applied at a distance of 1.1 m from one support, with a ratio a/d equal to 2.4. The load was applied by means of two hydraulic jacks acting on a rigid transverse steel beam, as shown in Figs. 6 and 7a, b.

According to the sketch reported in Fig. 6, four LVDTs were used to monitor specimen deflections: two of them were placed under the loading point (*F1*, *F2*), and the other two in correspondence of the supports (*FSA* and *FDA*), to detect possible boundary movements. In addition, 18 LVDTs characterized by different gauge lengths, ranging from 250 to 500 mm, were applied to each specimen, according to Fig. 6. More in details, five LVDTs were applied to HCS bottom (B1, B2, B3) and top (B1C, B3C) surfaces, while other eight were placed on the external webs, following the principal stress directions in compression (B6, B7, B10, B11)—approximately oriented at 30° with respect to slab longitudinal axis—and in tension

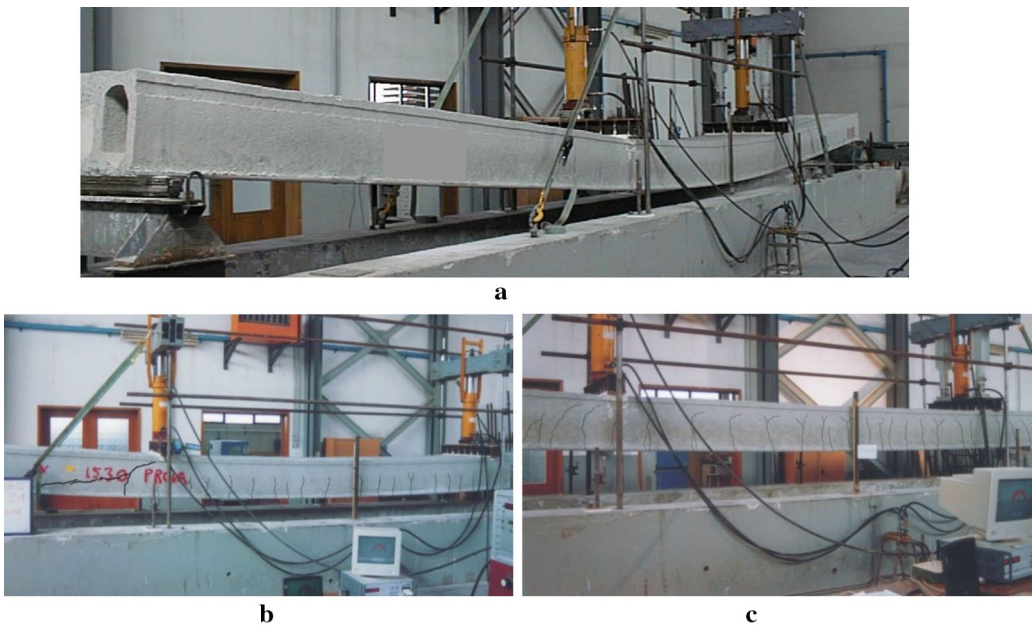

Fig. 5 Flexural tests: **a** specimen deflections at the end of the test; **b**, **c** experimental crack pattern in correspondence of the maximum applied load for slab H50-f1 and slab H50-f2, respectively.

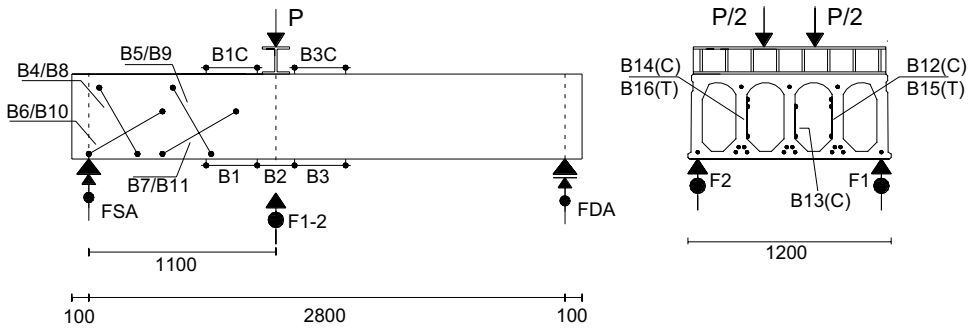

Fig. 6 Shear tests on specimens H50-s1 and H50-s2: sketch of the loading arrangement and of the instrumentation adopted for the measuring of strains and vertical displacements (dimensions in mm).

Fig. 7 Shear tests on specimens H50-s1 and H50-s2: **a**, **b** general view of the experimental setup; details of the adopted instrumentations; **c** view of LVDTs arrangement on HCS; **d** LVDTs arrangement inside hollows.

(B4, B5, B8, B9), see also Fig. 7c. In order to detect the shear crack evolution in internal HCS webs, the remaining 5 LVDTs were located inside the hollows, oriented along compression and tension isostatic lines (B12, B13, B14 and B15, B16, respectively, Fig. 7d).

The two shear tests were carried out under loading control, by performing two loading cycles.

In the first cycle, the load was incrementally applied until the attainment of the first cracking value P_{cr}, and then the HCS was unloaded. In the second cycle, after the removal of all the instrumentation for safety reasons, the specimen was loaded up to failure. On this point, it should be observed that in the first test (H50-s1) the main shear crack appeared during the first loading stage, when the instrumentation was still applied to the specimen, so determining an abrupt change in deflection and strain measurements (especially for those instruments directly interested by the spreading of cracks). In both the performed tests, specimen failure took place for a similar value of the applied load (equal to $P_{u,exp}=805$ kN for H50-s1, and $P_{u,exp}=841$ kN for H50-s2) and was characterized by the presence of a main diagonal crack spreading from the loading point to the support (Fig. 8), with an orientation approximately equal to 30°, as hypothesized for compression isostatic lines. This main shear crack first appeared in the inner webs of the HCS, and then propagated to the external ones, with a negligible change in its orientation, as can be observed in Figs. 8 and 9. The observed collapse mechanism was brittle and could be attributable to the shear tension failure of the web.

2.3 Material Characterization

2.3.1 Specimens H50-f1 and H50-f2

Concrete compressive and tensile strengths at the time of testing were determined on cubes and on cylindrical specimens made of the same mix as the HCS and subjected to the same curing conditions. The mean value of concrete compressive strength, obtained as the average strength of four cubes with 150 mm side, was equal to $f_{c,cube}=49.2$ MPa. The mean value of splitting tensile strength was obtained from four cylindrical specimens,

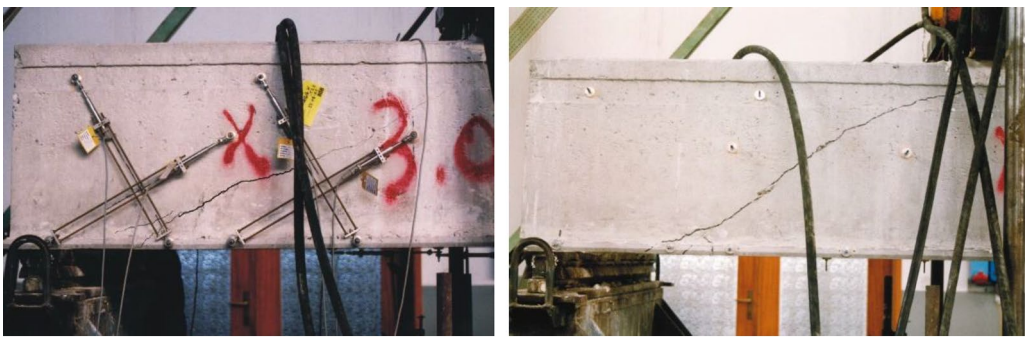

a **b**

Fig. 8 Shear tests: experimental crack pattern in correspondence of the ultimate applied load for **a** slab H50-s1 and **b** slab H50-s2.

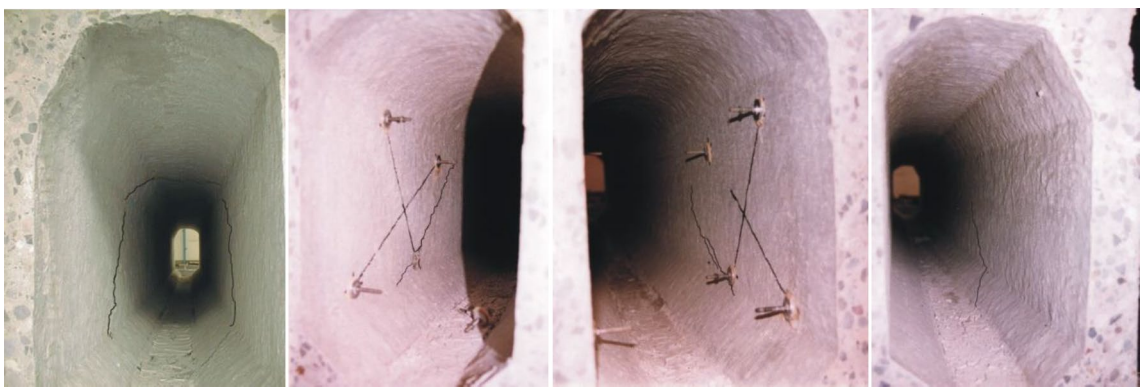

Fig. 9 Shear tests: experimental crack pattern registered inside the hollows of slab H50-s2, in correspondence of the ultimate applied load.

with diameter of 100 mm and height of 150 mm, and was equal to $f_{ct,sp}=4.0$ MPa.

However, it is known that mechanical properties of concrete in thin-walled sections are different from those specified on standard cubic samples (Flaga et al. 2016). Large differences may exist for the concrete tensile strength, which is important for determining the actual resistance of the element. For this reason, six prisms with 60 mm side and height equal to 200 mm, were extracted vertically from the central webs of the HCS at the end of the tests. These prisms were first subjected to three-point bending tests to determine their flexural strength and then each part of the broken specimens was tested in uniaxial compression. The obtained mean values of concrete strengths were respectively equal to $f_{ct,fl}=7.37$ MPa and $f_{c,pr}=45.64$ MPa, and so were similar to those determined on standard specimens.

Concrete properties are summarized in Table 1 for reading convenience.

2.3.2 Specimens H50-s1 and H50-s2

Mechanical properties of concrete were determined by performing compression tests on three 150 mm cubes, and splitting tests on three cylindrical specimens, characterized by a diameter equal to 100 mm and a height of 150 mm. All the specimens were cast at the same time as the HCS, and were subjected to the same curing conditions.

The mean values of concrete strengths obtained from the performed tests were respectively equal to $f_{c,cube}=54.7$ MPa and $f_{ct,sp}=4.4$ MPa, as also reported in Table 2.

3 Non-linear Finite Element Analysis of HCS

A high definition FE procedure was developed to explore the complex failure mechanisms of HCS. Numerical analyses were performed with a commercial FE software (ABAQUS), which allows to consider both mechanical and geometric non-linearity, even if the latter usually plays a weak role in the global response of HC elements. Besides material constitutive laws available in ABAQUS library, mechanical non-linearity can be included in numerical analyses by linking specifically conceived User-defined MATerial (UMAT) subroutines. In this work, 2D-PARC constitutive model, developed by some of the Authors in (Bernardi et al. 2016a, b; Cerioni et al. 2008) for RC elements subjected to plane stresses, was used to the scope. 2D-PARC model represents an effective alternative approach for the analysis of RC structures with respect to other constitutive models available in commercial programs. The proposed algorithm is indeed stable and has been successfully applied to the analysis of different types of structures (such as panels, beams, slabs, etc.…), allowing the prediction of the load-deformation response of each considered element up to its ultimate capacity.

The proposed procedure is here validated through the comparison between numerical results and experimental evidences coming from the flexural and shear tests described in Sect. 2.

3.1 Modelling Choices

The complex geometry of the panel cross-section, characterized by the presence of hollows, was modeled through a mesh of shell elements with different thickness, representing the middle plane of the webs, as well as the bottom and top slabs. More in detail, the creation of the FE mesh required the following steps, qualitatively sketched in Fig. 10: (1) individuation of the middle plane of HCS cross-section (Fig. 10a); (2) discretization of the transverse cross-section and evaluation of the equivalent average thickness to be attributed to each shell element (Fig. 10b); extrusion of the chosen discretization along HCS length. As an example, the resulting FE mesh adopted for the modelling of the HCS tested in shear is reported in Fig. 10c.

The possible presence of concrete fillings in some of the hollows was also taken into account in numerical simulations. These fillings are usually realized in current practice at slab ends or near floor openings, and were present only in the performed flexural tests (see Fig. 1b). To this end, in the corresponding FE mesh, vertical shell elements were added so to completely close the transverse cross-section of the filled hollows (see Fig. 10b). These shell elements were placed along the member axis direction in the portion of the panel interested by the presence of concrete fillings, and a proper shell thickness was attributed accordingly.

In detail, four-node, one-layered shell elements were adopted in the FE model. A Gauss reduced integration was applied in the shell plane, so to limit the required computational effort, while three Simpson integration points were considered through the element thickness, in order to get useful numerical results at the bottom and top surfaces. The choice of shell elements appears to be a good compromise, since it allows carrying out three-dimensional analyses, while using 2D-PARC constitutive model (whose formulation is referred to RC elements subjected to plane stresses).

Prestressing strands were included in the model by exploiting the ABAQUS "rebar layer" option (Fig. 11a). Each rebar (Fig. 11b) is schematized as a smeared layer hosted in the shell element (Fig. 11c). This smeared layer has a constant thickness equal to the area of the rebar divided by the reinforcement spacing. Each rebar is also characterized by its position along the shell thickness

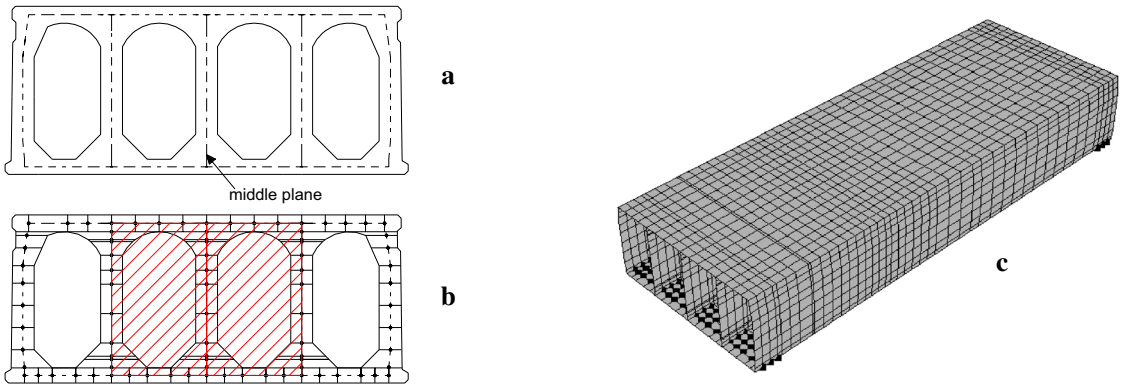

Fig. 10 FE model of HCS: **a** individuation of the middle plane of HCS cross-section; **b** cross section discretization, with vertical shell elements modeling concrete fillings (in red, for flexural tests only); **c** resulting mesh with shell elements adopted for specimens H50-s.

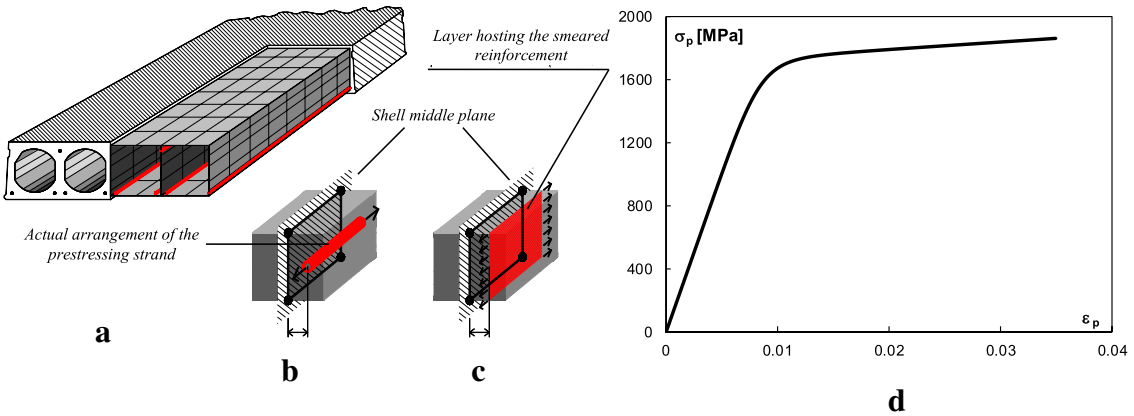

Fig. 11 **a** Modeling of prestressing strands through ABAQUS "rebar layer" option; **b** definition of rebar offset with respect to shell middle plane; **c** rebar layer smeared within the shell element; **d** elastic-hardening stress–strain law assumed in numerical analyses for prestressing steel.

(so to manage possible offset of strands with respect to the shell middle plane, i.e. Fig. 11b, c) and by its angular orientation with respect to the local axes of the shell element. The elastic-hardening constitutive law reported in Fig. 11d and calibrated on experimental strengths was assumed, while prestressing was assigned as not equilibrated initial condition in the first step of the numerical analysis. Final prestressing (after immediate and time dependent stress losses), as well as the corresponding transmission length to be inserted in the FE model were calculated according to Eurocode 2 (2015), under the assumptions described for analytical calculations in Sect. 4.2.1. A linear development of prestressing over the transmission length was considered. In slab end regions, the adopted FE mesh was also refined to allow a more gradual development of prestressing (Fig. 10c).

3.2 Inelastic Behavior of Concrete

The inelastic behavior of concrete was described through 2D-PARC model, which is a smeared, fixed crack formulation, implemented in the form of a secant stiffness matrix into ABAQUS. Both in the uncracked and in the cracked stage, concrete is treated as an orthotropic, nonlinear elastic material subjected to a general biaxial state of stress, following the approach described in Bernardi et al. (2016b) and based on the works of Ottosen (1979) and Ramaswamy et al. (1994).

After crack formation at a given integration point, a strain decomposition procedure is followed, by subdividing the total strain into two components respectively related to the strain of solid material between the cracks and to the strain of the crack (Cerioni et al. 2008). Local discontinuities are assumed to be smeared over a tributary volume within the FE and crack strain is expressed

as a function of the relative displacements of crack surfaces (i.e. opening and sliding). According to the basic hypothesis of fixed crack approaches, crack orientation remains fixed as loading increases, and is assumed as perpendicular to the direction of the principal tensile stress corresponding to crack initiation. In this way, normal and shear stresses exist on crack surfaces, and can be expressed as a function of the main resistant contributions. Due to the lack of ordinary reinforcement in HCS, the transmission of stresses across crack surfaces is in this case governed only by aggregate bridging and interlock, which are separately modelled according to the formulations discussed in Cerioni et al. (2008). The material stiffness matrix is then composed by combining crack contribution to that of undamaged concrete between two adjacent cracks, according to Cerioni et al. (2008).

4 Main outcomes of Numerical Analyses and Comparisons with Experimental Results

4.1 Flexural Tests

The main outcomes of numerical analyses relative to the flexural tests discussed in Sect. 2.1 are reported in Figs. 12, 13, 14, together with the corresponding experimental results, in terms of displacements, strains and crack pattern. As already discussed, experimental data are available only up to a loading level approximately corresponding to the attainment of the design flexural resistant moment (P_{MRd}, Fig. 4), since all the instrumentation was removed for safety reasons at the end of the 2nd loading cycle. Only midspan deflection was monitored almost to the end of the tests.

Figures 12a, b show the global response of the specimens, in terms of applied load P vs. midspan deflection f_c and vs. deflection under the loading point f_1, respectively. In both cases, the numerical curve reveals a good match with test results, being almost superimposed to the experimental ones. Numerical failure is assumed to happen in correspondence of the attainment of a strain limit value in concrete or in prestressing steel. In the examined case, the end of the dotted part of the curve corresponds to the achievement of tensile strength of prestressing steel, for a loading level almost equal to that corresponding to the end of jack stroke. The contour of longitudinal stresses in prestressing strands at numerical failure

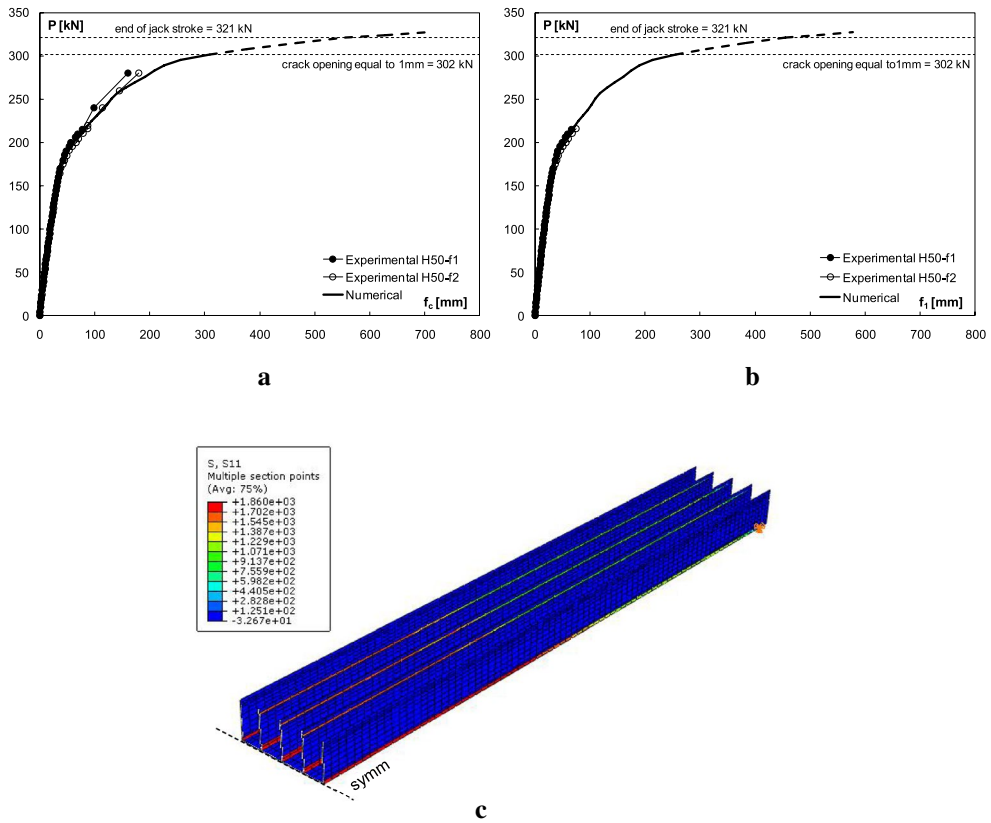

Fig. 12 Flexural tests on specimens H50-f1 and H50-f2: **a**, **b** comparisons between experimental and numerical results in terms of applied load P versus midspan deflection f_c and deflection under the loading point f_1 respectively; **c** longitudinal stress in prestressing reinforcement in correspondence of numerical failure.

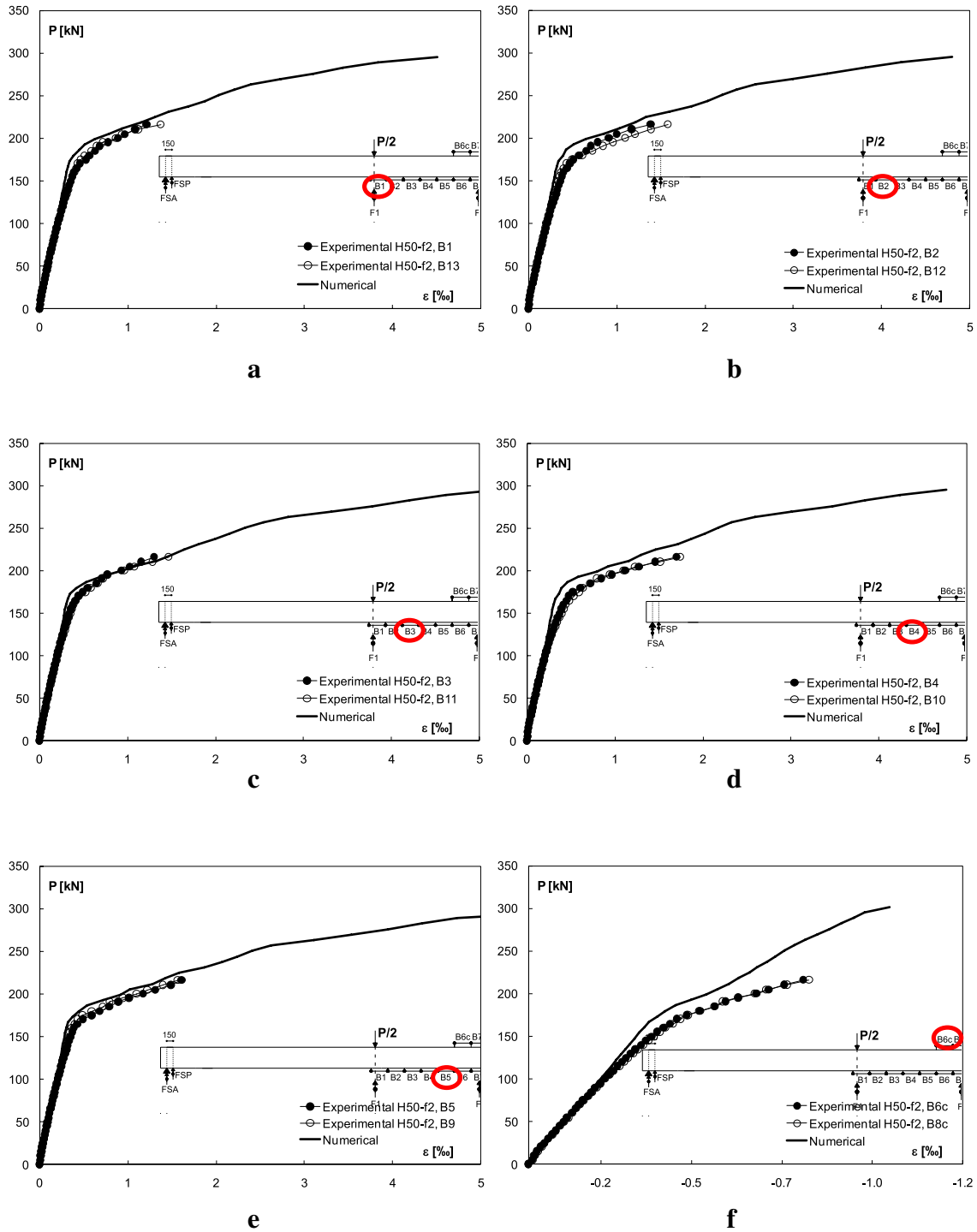

Fig. 13 Flexural tests: comparisons between experimental and numerical results for specimen H50-f2 in terms of applied load *P* versus strain *ε* obtained from devices **a** B1-B13, **b** B2-B12, **c** B3-B11, **d** B4-B10, **e** B5-B9, **f** B6c-B8c.

is plotted in Fig. 12c, which is referred to half specimen. The numerical failure load is slightly greater than that producing the attainment of the ultimate moment resistance M_{Rm}, calculated according to the assumptions of Eurocode 2 (2015) for sectional analysis, with mean values of material strengths and partial factors for

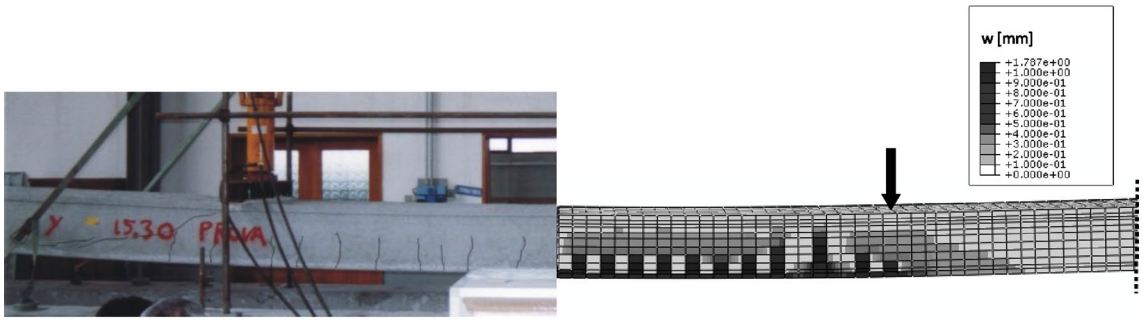

Fig. 14 Flexural tests: comparisons between numerical and experimental crack pattern registered at the end of H50-f1 test (w is the crack opening).

materials equal to 1. This ultimate moment, reduced by considering the flexure contribution due to element dead load—which acted before testing—corresponds to the application on the tested specimen of a load $P_{Rm} = 308$ kN (see also Fig. 4). However, by observing the attained numerical response, it can be seen that already after the reaching of a loading value almost equal to 302 kN (corresponding to end of the continuous curve and to the reaching of a crack opening $w = 1$ mm at the slab bottom surface), the numerical curve is characterized by a significant increase in slab deflections for little changes of the applied load. The deflection appears to be more than doubled (passing from 300 mm to more than 700 mm) for a loading increment of about 20 kN, highlighting a highly non-linear response, related to cracking development and strand deformations.

Numerical results are also satisfactory in terms of strain prediction, as can be seen from Fig. 13, which compares FE results with experimental data relative to specimen H50-f2 in terms of applied load P vs. strains ε measured at bottom and top surfaces, in the region of maximum bending moment. Experimental strain evolution with increasing loads is well caught from the FE model especially within the structure serviceability limit state, with a slight scatter only for the strains provided by measuring devices B6c, B8c, which are placed at slab top surface, closer to the midspan. However, given that the scale adopted for strains is smaller for this last graph (Fig. 13f), the comparisons can be still considered acceptable.

Finally, a comparison in terms of crack pattern corresponding to the final value of the experimental applied load is reported in Fig. 14.

4.2 Shear Tests

In case of shear tests, which are characterized by a sudden and brittle failure, it has been preferred to perform numerical analyses under displacement control, so to catch the peak load and the subsequent descending branch. To this end, the same displacement was applied to all those nodes lying on the upper slab of the HC unit and belonging to the considered loading section. This uniform displacement over the unit cross-section simulated the effect of the rigid transverse steel beam used for the redistribution of the applied load during the experimental test.

Some of the most interesting comparisons between numerical and experimental data are reported in Figs. 15, 16, 17, 18 in terms of displacements, strains and crack pattern at failure. Figure 15 shows HCS response in terms of applied load P vs. deflection under the loading point f_1. The adopted numerical model was able to catch the almost elastic-fragile capacity curve that is typical of deep HCS failing in shear, predicting with good accuracy the shear strength of the unit (it was found $P_{u,num}/P_{u,exp} = 1.06$

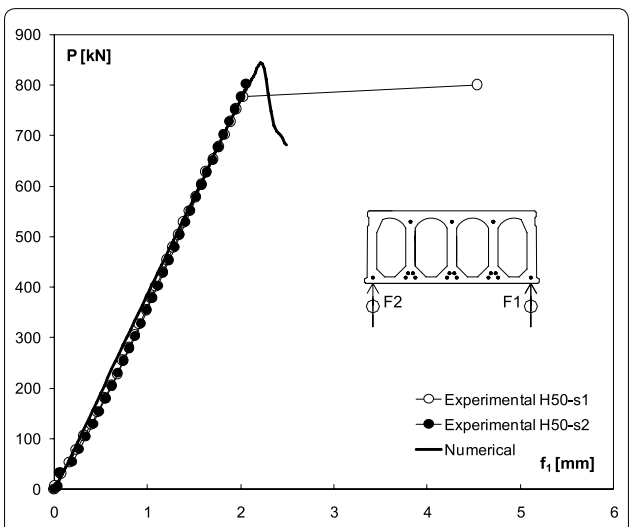

Fig. 15 Shear tests on specimens H50-s1 and H50-s2: comparisons between experimental and numerical results in terms of applied load P versus deflection under the loading point f_1.

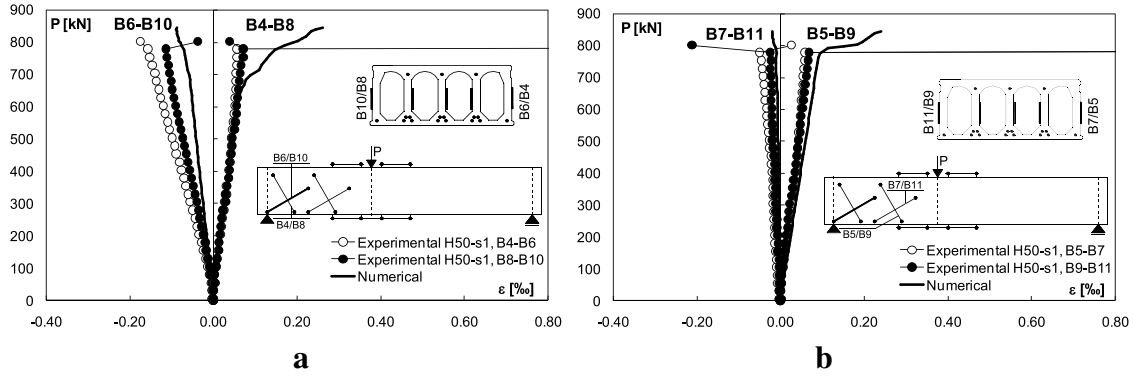

Fig. 16 Shear tests: comparisons between experimental and numerical results in terms of applied load *P* versus strain *ε* obtained from devices **a** B4-B8 (T) and B6-B10 (C); **b** B5-B9 (T) and B7-B11 (C) for specimen H50-s1.

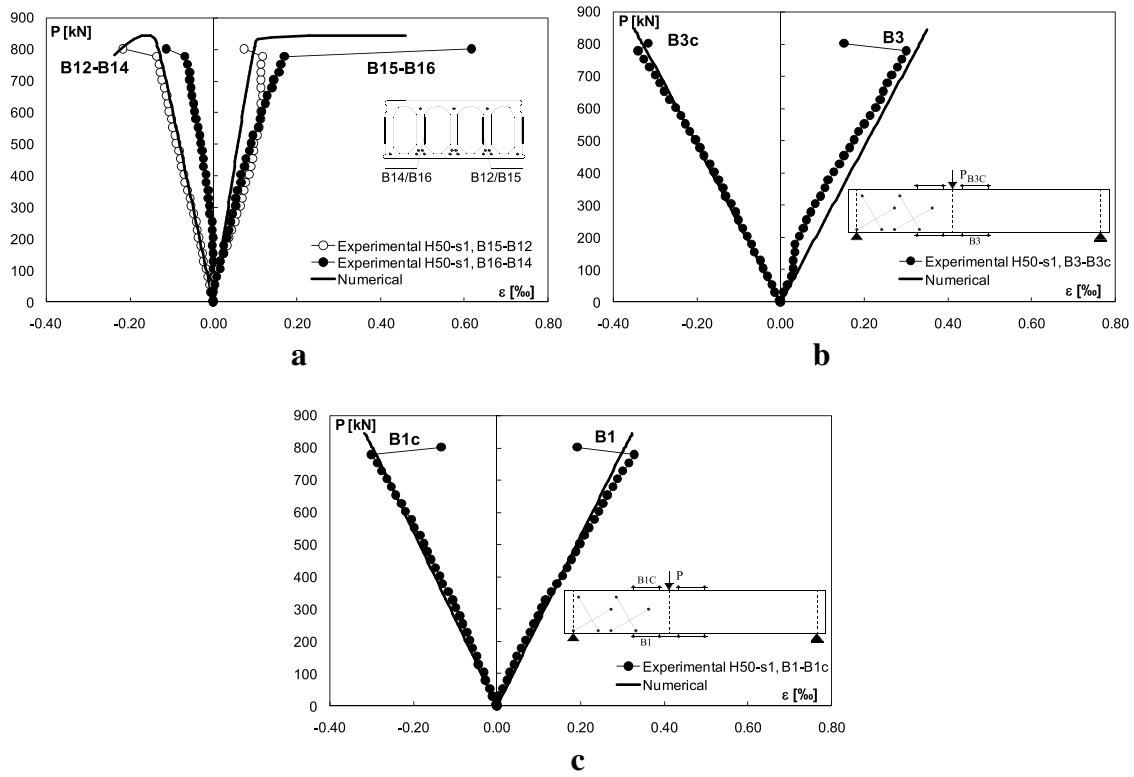

Fig. 17 Shear tests: comparisons between experimental and numerical results in terms of applied load *P* versus strain *ε* obtained from devices **a** B15-B16 (T) and B12-B14 (C); **b** B3 (T) and B3c (C); **c** B1 (T) and B1c (C) for specimen H50-s1.

for slab H50-s1 and $P_{u,num}/P_{u,exp} = 1.01$ for slab H50-s2, see Table 3).

The FE model was also able to simulate satisfactorily the strain field in the materials, as proved by the comparisons reported in Figs. 16 and 17, which are referred to some of the more interesting measuring device locations. Figure 16 is relative to strain measurements in correspondence of the external webs of the HCS, along the principal stress directions in compression (B6–B10, B7–B11) and in tension (B4–B8, B5–B9). The good match with experimental data proves that the proposed model is able to correctly predict the strain flow from the point of application of the transversely distributed line load and the support. This strain flow in turn is strictly

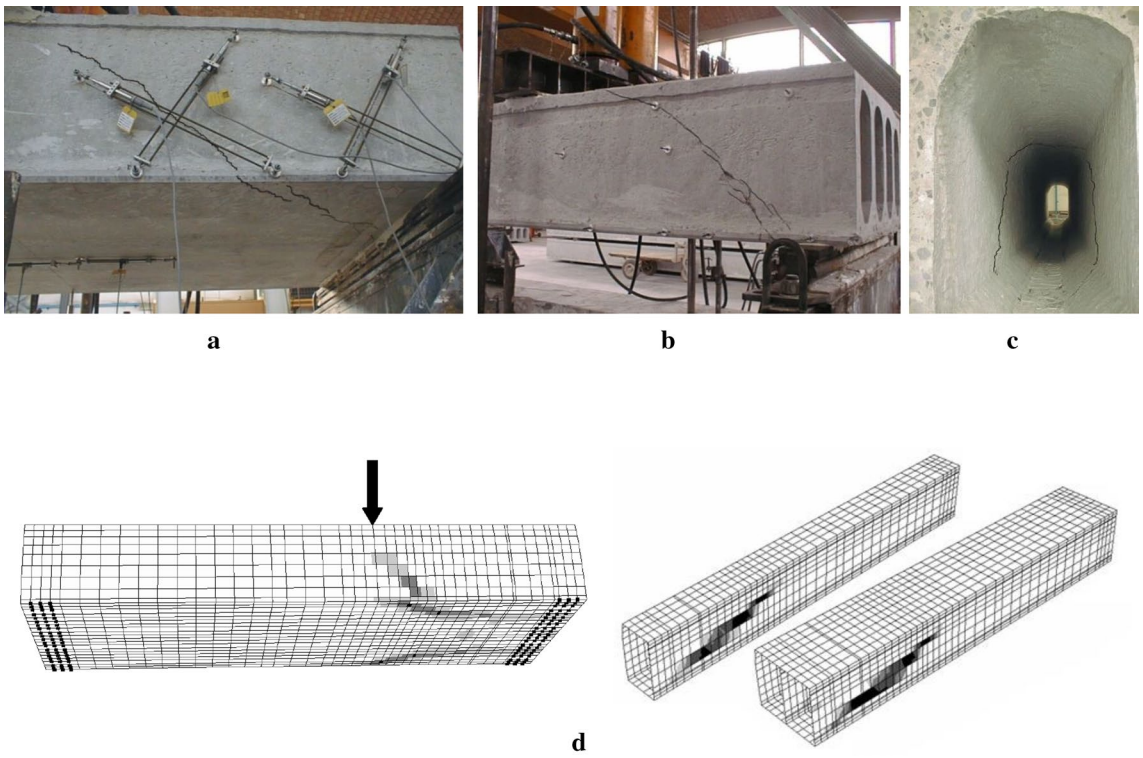

Fig. 18 Shear tests: comparison in terms of crack pattern at failure. Experimental crack pattern for **a** specimen H50-s1, and **b**, **c** specimen H50-s2; **d** crack distribution as obtained from the numerical model.

Table 3 Comparison between experimental, numerical and analytical results in terms of shear capacity for slabs H50-s1 and H50s-2.

Specimen	$P_{u,exp}$ (kN)	$P_{u,num}$ (kN)	P_{VRdc} (kN) (UNI EN 1168)	$P_{VRdc,mod}$ (kN) (Brunesi et al. 2015)	$P_{u,num}/P_{u,exp}$	$P_{VRdc}/P_{u,exp}$	$P_{VRdc,mod}/P_{u,exp}$
H50-s1	805	853.3	950.4	849.85	1.06	1.18	1.06
H50-s2	841				1.01	1.13	1.01

related to crack evolution and propagation through HCS depth. It should be observed that the experimental data registered for specimen H50-s1 from LVDTs in tension are meaningful only before the appearance of the main shear crack crossing the device length. Similarly, Fig. 17 is referred to the comparison between numerical predictions and experimental measurements in terms of strains in the hollow walls (Fig. 17a), as well as at slab bottom and top surfaces, both in the tension and in the compression region (Fig. 17b, c).

Finally, the efficiency of the numerical approach was checked in terms of prediction of the crack pattern at failure, as shown in Fig. 18. Similarly to experimental behavior, numerical failure was characterized by the appearance of a main inclined crack spreading from the loaded section to the support. Crack inclination showed a little change passing from internal to external webs of the HCS, and propagated also in the bottom slab of the unit (as also experimentally detected, see Fig. 18a). As also found by other researchers (see, e.g. Brunesi and Nascimbene 2015), crack inclination was fairly constant along the webs, due to the typical geometry of the cross-section of deep HCS, characterized by non-circular voids.

4.2.1 Additional Considerations on Shear Strength Prediction for Deep HCS

In HCS design, the shear strength in the region uncracked in bending is usually calculated according to the simplified relation suggested in UNI EN 1168 (2012):

$$V_{Rdc} = \phi \frac{I\, b_w}{S} \sqrt{\left(f_{ctd}\right)^2 + \beta\, \alpha_l\, \sigma_{cp}\, f_{ctd}} \quad (1)$$

where I is the moment of inertia of the section about the centroidal axis, S is the first area moment of the section about the centroidal axis, b_w is the web width, σ_{cp} is the concrete compressive stress at the centroid due to prestressing, and f_{ctd} is the design value of concrete tensile strength. ϕ is a reducing coefficient (equal to 0.8) introduced to overcome the fact that the peak shear stress may not be necessarily placed at the centroidal level, especially for deep cross-sections, as pointed out in the work of Yang (1994), while β is a reducing coefficient (equal to 0.9) referred to the transmission length. For HCS deeper than 450 mm, a further reduction of 10% of the shear—tension capacity V_{Rdc} obtained from Eq. (1), should be considered, as suggested by EN 1168 (2012). The calculation of the shear resistance according to Eq. (1) has to be carried out at the cross-section that lies at $h/2$ from the inner edge of the support.

To compare the analytical prediction of the shear strength with numerical and experimental results discussed in previous Sections, the mean value of concrete tensile strength $f_{ct,ax}$, according to Table 2, instead of the design value, is inserted in Eq. (1). Moreover, the transfer length l_{pt} (which is used for the evaluation of $\alpha_l = l_x/l_{pt2}$) is calculated according to Eurocode 2 (2015) assuming good bond conditions, gradual release of the prestressing tendons and a concrete tensile strength value equal to the one at the day of testing.

The so determined shear strength is equal to $V_{Rdc} = 577.05$ kN. The loading value corresponding to the attainment of this ultimate shear force, for the tested slab geometry and loading arrangement, is $P_{VRdc} = 950.44$ kN. As already pointed out, experimental failure took place for an applied load equal to $P_{u,exp} = 805$ kN for H50-s1, and $P_{u,exp} = 841$ kN for H50-s2, with a corresponding ratio between the predicted vs. observed shear resistance equal to 1.18 and 1.13, respectively (see Table 3). The analytical values obtained from UNI EN 1168 (2012) are still on the unsafe side, despite all the reducing factors introduced in Eq. (1) to take into account the specific features of deep HCS with non-circular voids. A better analytical prediction can be instead obtained from Eq. (1), by posing $\phi = \beta = 1$ and introducing the reducing coefficient $1/C_s$ proposed by Brunesi and Nascimbene (2015) to account for the effects of cross-section geometry on shear failure. According to their work, C_s can be calculated as:

$$C_s = C_1 \frac{b_1}{r} \cdot C_2 \frac{h_3}{r} \cdot C_3 \frac{b_2}{b_1}$$

where b_1/r is the horizontal distance between the webs normalized by the void radius, h_3/r measures the constant web width stretch along the depth and b_2/b_1 quantifies the suddenness of the web width drop (see Brunesi and Nascimbene 2015 for further details). C_1, C_2 and C_3 are best-fitting coefficients, assumed equal to 1.1, 1 and 1.15, respectively, as suggested by the Authors. Following this approach, the external load corresponding to shear failure results $P_{VRdc,\ mod} = 849.85$ kN, which is almost equal to the value provided by numerical simulations performed in this work. It should be underlined that this calculation was done by neglecting the further reduction of 10% of the shear strength suggested by Product Standard for deep sections, otherwise a more conservative prediction is obtained.

5 Conclusions

The paper discusses the main results of an experimental and numerical research on precast prestressed deep HCS subjected to flexure and shear. The work was structured in two main phases:

1. execution of 4 experimental tests on a 500 mm deep HCS (two in flexure and two in shear)
2. validation of the adopted numerical procedure, which takes into account the material non-linearity by means of 2D-PARC model, through a detailed comparison with experimental results.

Numerical and experimental results were also compared with analytical formulations available in the Product Standard and in the literature for the prediction of shear resistance, which is quite critical for these elements without shear reinforcement, especially in case of deep sections with non-circular voids.

The obtained results prove that the adopted numerical procedure, based on fracture mechanics principles, represents a rational technique for analyzing cracking development and propagation in deep HCS. The numerical prediction of shear strength is almost coincident with that obtained by applying the semi-analytical relation suggested by Brunesi and Nascimbene (2015), which is in turn based on complex FE analyses, carried out with a different technique. Thanks to its reliability, the proposed procedure can be regarded as an interesting approach for studying not only a single HCS, but also whole HC floors, even in presence of complex geometries or not trivial loading and/or boundary conditions (e.g. irregular floor plans, presence of openings, concentrated loads, and presence of supports or fixed joints). Numerical results could be then returned in the form of correction coefficients or design charts to be used in current design practice. These design tools can be adopted for correcting the results of standard beam-like calculations on single HCS, similarly to what already proposed by the Authors for other precast prestressed elements (Belletti et al. 2015; Bernardi et al. 2020).

Acknowledgements
The authors gratefully acknowledge ASSAP (Italian Prestressed Hollow Core Slabs Manufacturers Association) for supporting the research work and allowing the publication of the results. The authors also thank Ph.D. Eng. Nicola Garutti for his valuable help in numerical analyses.

Authors' contributions
All authors contributed equally to this paper. All authors read and approved the final manuscript.

Authors' information
E. M., Ph.D., Assistant Professor in Structural Engineering, Department of Engineering and Architecture, University of Parma, Parma, Italy. P. B., Ph.D., Assistant Professor in Structural Engineering, Department of Engineering and Architecture, University of Parma, Parma, Italy. R. C., Full Professor in Structural Engineering, Department of Engineering and Architecture, University of Parma, Parma, Italy. B. B., Ph.D., Associate Professor in Structural Engineering, Department of Engineering and Architecture, University of Parma, Parma, Italy.

Funding
The authors received no specific funding for this work.

Availability of data and materials
The experimental data used to support the observations of this study are included in the article.

Competing interests
The authors declare that they have no competing interests.

Received: 31 December 2019 Accepted: 25 March 2020
Published online: 07 July 2020

References

ACI Committe. (2011). *Building code requirements for structural concrete (ACI 318-11) and commentary*. Farmington Hills, MI: American Concrete Institute.

Araujo, C. A. M., Loriggio, D. D., & Da Camara, J. M. M. N. (2011). Anchorage failure and shear design of hollow-core slabs. *Structural Concrete, 12,* 109–119.

Baran, E. (2015). Effects of cast-in-place concrete topping on flexural response of precast concrete hollow-core slabs. *Engineering Structures, 98,* 109–117.

Belleri, A., Brunesi, E., Nascimbene, R., Pagani, M., & Riva, P. (2015). Seismic Performance of Precast Industrial Facilities Following Major Earthquakes in the Italian Territory. Journal of Performance of Constructed Facilities. 04014135.

Belletti, B., Bernardi, P., Cerioni, R., & Iori, I. (2003). Non-linear analysis of pre-stressed hollow core slabs. In Proc. of the 2nd International Congress on Structural and Construction Engineering, Rome, Italy, Sep 23–26, 1–3.

Belletti, B., Bernardi, P., & Michelini, E. (2015). Behavior of thin-walled prestressed concrete roof elements—Experimental investigation and numerical modeling. *Engineering Structures, 107,* 166–179.

Belletti, B., Cerioni, R., & Iori, I. (2001). Physical approach for reinforced-concrete (PARC) membrane elements. *Journal of Structural Engineering, 127*(12), 1412–1426.

Belletti, B., Franceschini, L., & Ravasini, S. (2019). Tie Force Method for Reinforced Concrete Structures. In *Proc. of International fib Symposium on Conceptual Design of Structures*, *Madrid, Spain, Sept 26–28.*

Belletti, B., Scolari, M., & Vecchi, F. (2017). PARC_CL 2.0 crack model for NLFEA of reinforced concrete structures under cyclic loadings. *Computer and Structures, 191,* 165–179.

Bernardi, P., Cerioni, R., Leurini, F., & Michelini, E. (2016a). A design method for the prediction of load distribution in hollow-core floors. *Engineering Structures, 123,* 473–481.

Bernardi, P., Cerioni, R., Michelini, E., & Sirico, A. (2016b). Numerical modeling of the cracking behavior of RC and SFRC shear-critical beams. *Engineering Fracture Mechanics, 167,* 151–166.

Bernardi, P., Cerioni, R., Michelini, E., & Sirico, A. (2020). Transverse reinforcement optimization of a precast special roof element through an experimental and numerical procedure. *Engineering Structures, 203,* 109894.

Bertagnoli, G., & Mancini, G. (2009). Failure analysis of hollow-core slabs tested in shear. *Structural Concrete, 10,* 139–152.

Broo, H. (2008). Shear and torsion in concrete structures—Non-linear finite element analysis in design and assessment. PhD thesis, Chalmers University of Technology, Goteborg, Sweden.

Broo, H., Lundgren, K., & Engstrom, B. (2007). Shear and torsion in prestressed hollow core units: finite element analyses of full-scale tests. *Structural Concrete, 8,* 87–100.

Brunesi, E., Bolognini, D., & Nascimbene, R. (2015). Evaluation of the shear capacity of precast-prestressed hollow core slabs: Numerical and experimental comparisons. *Matererials and Structures, 48,* 1503–1521.

Brunesi, E., & Nascimbene, R. (2015). Numerical web-shear strength assessment of precast prestressed hollow core slab units. *Engineering Structures, 102,* 13–30.

CEB-FIP. (2000). fib Bulletin No. 6—Special design considerations for precast prestressed hollow core floors, Guide to good practice. Fédération Internationale du Béton, Lausanne, Switzerland.

Cerioni, R., Iori, I., Michelini, E., & Bernardi, P. (2008). Multi-directional modeling of crack pattern in 2D R/C members. *Engineering Fracture Mechanics, 75,* 615–628.

Dal Lago, B. (2017). Experimental and numerical assessment of the service behaviour of an innovative long-span precast roof element. *International Journal of Concrete Structures and Materials, 11,* 261–273.

Derkowski, W., & Surma, M. (2015a). Composite action of precast hollow core slabs with structural topping. *Czasopismo Techniczne, 2015,* 15–29.

Derkowski, W., Surma, M. (2015b). Complex stress state in prestressed hollow core slabs. Recent advances in civil engineering: building structures, Cracow University of Technology.

Duthinh, D. (1999). Sensitivity of shear strength of reinforced concrete and prestressed concrete beams to shear friction and concrete softening according to modified compression field theory. *Structural Journal, 96,* 495–508.

Elliot, S. K. (2002). *Precast concrete structures*. Oxford: Butterworth-Heineman.

El-Sayed, A. K., Al-Negheimish, A. I., & Alhozaimy, A. M. (2019). Web shear resistance of prestressed precast deep hollow core slabs. *ACI Structural Journal, 116,* 139–150.

Flaga, K., Derkowski, W., & Surma, M. (2016). Concrete strength and elasticity of precast thin-walled elements. Cement Wapno Beton 5.

Garutti, N. (2013). Numerical analysis of the structural behavior of HC floors in presence of openings (in Italian), Ph.D. dissertation, University of Parma, Italy.

Girhammar, U. A., & Pajari, M. (2008). Tests and analysis on shear strength of composite slabs of hollow core units and concrete topping. *Construction and Building Matererials, 22,* 1708–1722.

Hegger, J., Roggendorf, T., & Kerkeni, N. (2009). Shear capacity of prestressed hollow core slabs in slim floor constructions. *Engineering Structures, 31,* 551–559.

Ibrahim, I. S., Elliott, K. S., Abdullah, R., Kueh, A. B. H., & Sarbini, N. N. (2016). Experimental study on the shear behaviour of precast concrete hollow core slabs with concrete topping. *Engineering Structures, 125,* 80–90.

Ibrahim, I. S., Elliott, K. S., & Copeland, S. (2008). Bending capacity of precast prestressed hollow core slabs with concrete toppings. *Malaysian Journal of Civil Engineering, 20,* 260–283.

Lam, D., Elliott, K. S., & Nethercot, D. A. (2000). Experiments on composite steel beams with precast concrete hollow core floor slabs. *Proceedings of the Institution of Civil Engineers-Structures and Buildings, 140,* 127–138.

Lundgren, K., Broo, H., & Engstrom, B. (2004). Analyses of hollow core floors subjected to shear and torsion. *Structural Concrete, 5,* 161–172.

Nguyen, T. N. H., Tan, K.-H., & Kanda, T. (2019). Investigations on web-shear behavior of deep precast, prestressed concrete hollow core slabs. *Engineering Structures, 183,* 579–593.

Ottosen, N. S. (1979). Constitutive model for short-time loading of concrete. *Journal of the Engineering Mechanics Division ASCE, 105,* 127–141.

Pajari, M. (2005). Resistance of prestressed hollow core slabs against web shear failure. ESPOO 2005, VTT Research Notes 2292.

Pajari, M. (2009). Web shear failure in prestressed hollow core slabs. *Journal of Structural Engineering, 42,* 207–217.

Palmer, K. D., & Schultz, A. E. (2011). Experimental investigation of the web-shear strength of deep hollow-core units. *PCI Journal, 56,* 83–104.

Park, M.-K., Lee, D. H., Han, S.-J., & Kim, K. S. (2019). Web-shear capacity of thick precast prestressed hollow-core slab units produced by extrusion method. *International Journal of Concrete Structures and Materials, 13,* 7.
Pisanty, A., & Regan, P. E. (1991). Direct assessment of the tensile strength of the web in prestressed precast hollow-core slabs. *Matererials and Structures, 24,* 451–455.
Prakashan, L. V, George, J., Edayadiyil, J.B., & George, J.M. (2017). Experimental study on the flexural behavior of hollow core concrete slabs. In Applied mechanics and materials, Trans Tech Publ, p. 107–112.
Rahman, M. K., Baluch, M. H., Said, M. K., & Shazali, M. A. (2012). Flexural and shear strength of prestressed precast hollow-core slabs. *Arabian Journal for Science and Engineering, 37,* 443–455.
Ramaswamy, B. A., Barzegar, F., & Voyiadjis, G. Z. (1994). Postcracking formulation for analysis of RC structures based on secant stiffness. *Journal of Engineering Mechanics, 120,* 2621–2640.
Rots, J.G. (1988). Computational modeling of concrete fracture. Ph.D. Dissertation, Delft University of Technology, The Netherlands.
Savoia, M., Buratti, N., & Vincenzi, L. (2017). Damage and collapses in industrial precast buildings after the 2012 Emilia earthquake. *Engineering Structures, 137,* 162–180.
Sgambi, L., Gkoumas, K., & Bontempi, F. (2014). Genetic algorithm optimization of precast hollow core slabs. *Computers and Concrete, 13,* 389–409.
Simasathien, S., & Chao, S.-H. (2015). Shear strength of steel-fiber-reinforced deep hollow-core slabs. *PCI Journal, 60,* 85–101.
Song, J.-Y., Elliott, K. S., Lee, H., & Kwak, H.-G. (2009). Load distribution factors for hollow core slabs with in-situ reinforced concrete joints. *International Journal of Concrete Structures and Materials, 3,* 63–69.
Tawadrous, R., & Morcous, G. (2018). Shear strength of deep hollow-core slabs. *ACI Structural Journal, 115,* 699–709.
Ueda, T., & Stitmannaithum, B. (1991). Shear strength of precast prestressed hollow slabs with concrete topping. *Structutal Journal, 88,* 402–410.
UNI EN 1168. (2012). Precast concrete products—Hollow core slabs.
UNI EN 1992-1-1. (2015). Eurocode 2—Design of concrete structures—Part 1-1 : General rules and rules for buildings.
Walraven, J. C., & Mercx, W. P. M. (1983). The bearing capacity of prestressed hollow core slabs. *HERON, 28*(3), 1983.
Wang, X. (2007). Study on the shear behavior of prestressed concrete hollow core slabs by nonlinear finite element modelling. Ph.D. Dissertation, University of Windsor, Windsor, Canada.
Yang, L. (1994). Design of prestressed hollow core slabs with reference to web shear failure. *ASCE Journal of Structural Engineering, 120,* 2675–2696.

Publisher's Note